Biomed Microdevices (2009) 11:1091–1101
DOI 10.1007/s10544-009-9326-4

Neuronal cell biocompatibility and adhesion to modified CMOS electrodes

Anthony H. D. Graham · Chris R. Bowen · John Taylor · Jon Robbins

Published online: 21 May 2009

Abstract The use of CMOS (Complementary Metal Oxide Semiconductor) integrated circuits to create electrodes for biosensors, implants and drug-discovery has several potential advantages over passive multi-electrode arrays (MEAs). However, unmodified aluminium CMOS electrodes may corrode in a physiological environment. We have investigated a low-cost electrode design based on the modification of CMOS metallisation to produce a nanoporous alumina electrode as an interface to mammalian neuronal cells and corrosion inhibitor. Using NG108-15 mouse neuroblastoma x rat glioma hybrid cells, results show that porous alumina is biocompatible and that the inter-pore distance (pore pitch) of the alumina has no effect on cell vitality. To establish whether porous alumina and a cell membrane can produce a tight junction required for good electrical coupling between electrode and cell, we devised a novel cell detachment centrifugation assay to assess the long-term adhesion of cells. Results show that porous alumina substrates produced with a large pore pitch of 206 nm present a significantly improved surface compared to the unmodified aluminium control and that small pore-pitches of 17 nm and 69 nm present a less favourable surface for cell adhesion.

A. H. D. Graham (✉) · J. Taylor
Department of Electronic & Electrical Engineering,
University of Bath,
Bath BA2 7AY, UK
e-mail: abmahdg@bath.ac.uk

C. R. Bowen
Department of Mechanical Engineering, University of Bath,
Bath BA2 7AY, UK

J. Robbins
Receptors & Signalling, Wolfson CARD, King's College London,
London SE1 1UL, UK

Keywords Biocompatibility · Adhesion · Neuron · Electrode · CMOS · Porous alumina

1 Introduction

Multi-electrode arrays (MEAs) are an established platform for *in vitro* recording and stimulation of neuronal cells, either as tissue slices or dissociated cells. Commercial MEA products are available, but manufacturing relies on access to specialised microfabrication equipment, in particular for photolithography. The complexity of MEA manufacture is reflected in the high cost, with a single reusable 8×8 electrode array presently costing roughly £350 (€420) in the UK. This constrains the market to low-volume applications such as electrophysiology research devices and implants.

Relatively simple electrodes have been used in commercially successful implantable medical devices (IMDs) to assist in the diagnosis, management and restoration of nervous system disorders (Donoghue et al. 2007). Successful applications are primarily within functional electrical stimulation (FES) neuroprosthetics such as the pacemaker, 'Dropped Foot' stimulator, bladder control (e.g. Interstim®), cochlear implants (e.g. from Med-El and Advanced Bionics) and paralysed muscle reanimation (e.g. BION® from the Alfred Mann Institute). Implants using more sophisticated electrode arrays, incorporating recording as well as stimulation electrodes, are only at an early stage of development.

A further potential application of electrode arrays is in drug discovery assays whereby electrophysiological activity can be monitored through MEAs embedded within the base of each well of a microtitre plate (Ressler et al. 2004). With a single assay consisting of many plates, typically each with

384 wells, the cost of embedding custom-fabricated MEAs becomes prohibitive. A further problem arises when considering the connection of each electrode to recording circuitry. With 'passive' devices — those with no supporting electronic circuitry — each electrode requires a connection to the plate edge. For example, a 384 well plate with each well containing an array of 64 electrodes would require 24,576 connections at the plate edge. These limitations can be overcome by combining electrodes with other signal-processing circuitry on integrated circuits (ICs), the most widely available and low-cost form of which is silicon CMOS (Complementary Metal Oxide Semiconductor). The most common approach to forming electrodes using CMOS stems from the premise of creating openings through the surface of the IC insulating and protection layer (the passivation) down to the underlying metal used for interconnects. With mature CMOS processes that are readily available for these applications, the interconnect metal is commonly an alloy of aluminium.

However, previous work in this field has been concerned with the neurotoxicity associated with aluminium and has therefore sought to modify the CMOS electrodes. Heer et al. (2007) have succeeded in producing a biocompatible array by introducing additional deposition and photolithography steps to the CMOS process to create platinum electrodes shifted away from the openings to the aluminium (pads). Due to the high cost of the microfabrication apparatus required to create these shifted electrodes, this approach is most suited to low volume research platforms. Berdondini et al. (2004) introduced a low-cost approach of electroless plating of aluminium pads with gold. However, in physiological medium, the electrode could be susceptible to galvanic corrosion between the noble gold plating and the electronegative aluminium (Dini 1993; Virtanen et al. 2008).

In this paper we seek alternative designs for a low-cost CMOS electrode. To provide context for our research it is important to define the key criteria for the development of such an electrode, namely biocompatibility, good cell adhesion to the substrate, electrochemical stability in a biological environment and adequate electrical performance.

Biocompatibility The biocompatibility of aluminium and its oxide, alumina, have been thoroughly studied, much work having being done to evaluate *in vivo* performance of alumina for use with orthopaedic prosthetics (Ravaglioli and Krajewski 1992; Williams 1981). The performance of aluminium metal depends much on the adherent superficial (native) oxide layer. Brinton et al. (2005) found that growth of hippocampal neurons on aluminium was 'excellent' with cells remaining adhered for several weeks. Similar results for epithelial cells were reported by Bogner et al. (2006). However, the *in vivo* use of alumina has generally been confined to orthopaedics because of the metal's poor compatibility with blood due to its thrombogenic action, as a result of which aluminium prosthetics are frequently coated with titanium nitride to improve performance.

Cell-substrate adhesion It has been found that nanoporous morphologies may form good substrates for CMOS electrodes (Bayliss et al. 2000; Low et al. 2006). In Sapelkin et al. (2006) a CMOS IC was etched to form porous silicon (pSi) which was found to be biocompatible with good cell adhesion. Johansson et al. (2008) showed axons preferred to grow on pSi with medium pore sizes (150–500 nm) rather than smooth silicon or pSi with larger (1500 nm) or smaller (100 nm) pores. Unfortunately, access to the silicon substrate on standard CMOS technology is only possible by etching through the passivation, metal and insulation layers. This also exposes the active (transistor) regions of the IC to the physiological medium which will then cause rapid degradation of the circuits due to ionic contamination (Sabnis 1990). In Moxon et al. (2004) the use of pSi in fabricated MEA electrodes confirmed that the nano-porous electrode surface was more biocompatible than a smooth silicon surface, illustrated by the increased growth of neurites and the reduced adhesion of astrocytes (glial cells).

Electrochemical stability The overall interaction of a prosthetic with its environment is primarily governed by the natural chemistry of the body: simplistically, this is a NaCl aqueous solution of concentration ~0.1 M with organic acids, proteins, enzymes, macromolecules, electrolytes, dissolved oxygen and nitrogenous compounds. The resulting pH is approximately 7.2, often decreasing to ~5.5 in the vicinity of tissue damage and/or infection. The degradation of the thin (~10 nm) aluminium native oxide in a physiological environment is limited by its natural corrosion resistance. However, a concern is that either defects in the oxide film may enable aluminium ions to leach into the body or that the alumina itself may degrade. In physiological conditions aluminium easily forms an insoluble $Al(OH)_3$ precipitate or a solution of $AlCl_3$. The toxicity of these and other aluminium salts (10 – 100 mM) has been evaluated and shown to have only a small effect on the viability of mammalian neuronal cells (Kawahara et al. 2001). Aluminium has also been associated with the pathogeny of Alzheimer's Disease, but a causal relationship has not been demonstrated (Perl and Moalem 2006). However, due to these concerns, Walpole et al. (2003) and Karlsson et al. (2003) tested nano-porous alumina substrates for aluminium ion leakage and they concluded that the dissolution of ions into the culture was not toxic.

Electrical performance To ensure sufficient extracellular signal is recorded, it has been shown by Fromherz (2003) that a neuron should be in intimate contact with the

electrode surface so that the gap between the underside of the cell and electrode — the 'cleft' — is minimised. This prevents loss of extracellular signal caused by leakage laterally along the cleft to the extracellular medium beyond the vicinity of the cell-electrode interface. It has been shown that coating the electrode with large cell adhesion molecules increases the cleft whereas coating with short peptide sequences such as YIGSR (the single letter codes for the amino acid sequence) may reduce the cleft (Schoen and Fromherz 2007). Extracellular adhesion proteins and the glycocalyx will also contribute to the cleft (Bongrand 1995). Practical methods have been developed to quantify the cleft magnitude such as fluorescence interference contrast (FLIC) (Sorribas et al. 2001), tunnelling electron (Wrobel et al. 2008) and focussed ion beam microscopy (Greve et al. 2007). However, to understand the intrinsic nature of the porous alumina surface we have chosen to study the alumina in the absence of such organic coatings.

Our preliminary observations (Graham et al. 2009) showed that corrosion of aluminium CMOS pads is indeed problematic and therefore requires modification of the electrode to prevent degradation. We proposed that conversion of the CMOS aluminium pads to porous alumina may prevent corrosion by creating bioinert alumina at the interface and at the same time consuming the bulk of the aluminium thus eliminating the corrosion source. The proposed electrode is illustrated in Fig. 1(a), showing a typical CMOS IC with 'pad' openings to form electrodes, i, on the uppermost of the metal layers (four layers shown in this example), with passivation layer, ii, and transistor area within the silicon substrate, iii. Cells, iv, are cultured on the surface of the IC. Figure 1(b) is an enlarged view showing the electrode area converted to porous alumina, v, with an adherent cell membrane, vi, forming a seal with the top of the pores with a cleft, vii. In this basic configuration, electrical connection is made via the remaining conductive layer, viii, below the porous alumina. Other configurations could include an electrodeposition of a noble metal into the pores which would decrease the impedance and change the cell-substrate interface. The resulting electrical performance, described further in Section 4, has yet to be proven.

The height of the pores is determined by the proportion of the CMOS aluminium layer that is anodised, the maximum being ~1 μm representing the full thickness of the metal. The inter-pore spacing (usually termed 'cell size' but to avoid confusion shall here be referred to as 'pore pitch') is also selectable and is determined by the anodisation voltage. We have produced a range of substrates for evaluation with mean pore pitches of 17 nm (anodised at 10 V) to 206 nm (120 V).

In this paper we evaluate the biocompatibility of the porous alumina electrode surface and also evaluate whether a porous morphology provides good cell adhesion. Neuronal cells have previously been cultured on porous alumina, but data from the literature are difficult to apply to the context we are studying, i.e. evaluation of the intrinsic nature of an uncoated porous alumina surface and with substrates configured in a manner that is conducive to subsequently forming an electrode such as closed conductive substrate rather than membrane (Prasad and Quijano 2006; Wolfrum et al. 2006). Others have evaluated non-neuronal cell types on porous alumina, in particular osteoblasts, and shown good biocompatibility (Walpole et al. 2003; Karlsson et al. 2003; Leary Swan et al. 2005; Hoess et al. 2007; Karlsson et al. 2004). The objectives of our experiments were therefore to, firstly, evaluate the biocompatibility with neuronal cells of porous alumina configured in a manner compatible with CMOS processing and, secondly, to characterise adhesion versus alumina pore pitch.

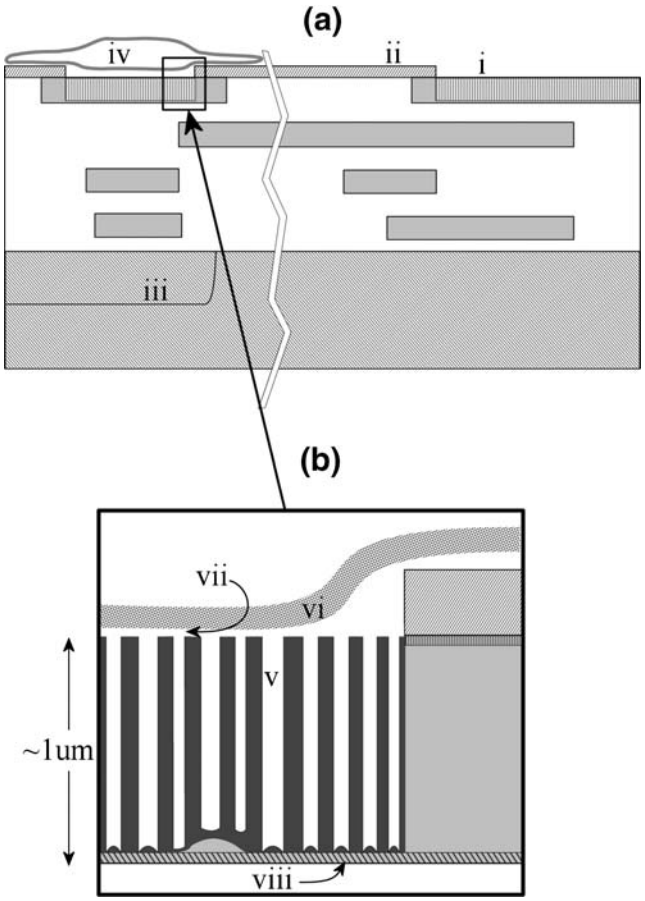

Fig. 1 Electrode arrangement: (**a**) Section of a typical CMOS IC showing 'pads', i, as openings in the passivation layer, ii. Transistor area, iii, is within the silicon substrate. Cells, iv, are cultured on the surface of the IC; (**b**) Enlarged view, with porous alumina, v, cell membrane, vi, cleft, vii, and electrical connection to amplifier, viii

Tests for cell-substrate adhesion Cell vitality tests give little indication as to whether a cell is bound to a surface or is detached (Mayne et al. 2000). Whether it is chosen to

coat with adhesion molecules or not, good electrical coupling always requires cells to be adhered to the electrode surface. A variety of adhesion assays have been developed, including the parallel-plate flow chamber, rotating disk (Cargill et al. 1999), jet impingement (Giliberti et al. 2002) and centrifugation.

A flow chamber design has already been developed specifically for the measurement of NG108-15 cells (Schneider et al. 2001). Expected shear stress magnitudes are therefore already understood for this cell line.

We developed a flow chamber based on the designs of Schneider et al. (2001) and Kaper et al. (2003), but with a recess in the base to hold the coverslip substrates. Most usefully, the flow chamber allows real-time microscopy of the substrates using an epi-illumination microscope allowing the detachment of individual cells to be observed. However, preliminary adhesion tests using this apparatus (unpublished data) revealed two limitations. Firstly, we are interested in measuring the long-term adhesion of the cells on a working electrode (several days to weeks) rather than the short-term adhesion processes (hours) that are usually evaluated using a flow chamber. Adhesion strengths greatly increase over several days *in vitro* (Gallant and García 2007) and flow chambers can then no longer provide sufficient laminar flow to cause detachment. Shear strength may again decrease to measurable levels for cells plated for extended durations and so show loss of vitality, but this is of little interest in the context of electrophysiology. Secondly, we observed that under high flow the stain (see below) leached from the cells causing subsequent difficulty in detecting those cells that remain adhered.

2 Methods

Using functional MEAs to evaluate the cell-substrate interactions is inefficient since only a small proportion of the substrate surface is electrode. It was therefore decided to reproduce the electrode surface on glass microscope coverslips. The 22×32 mm coverslips were coated to reproduce closely a typical CMOS metallisation by depositing ~40 nm of titanium onto the coverslip followed by approximately 960 nm of aluminium (Teer Coatings Ltd, UK). It should be noted that titanium nitride anti-reflective coatings — often used on CMOS processes — are removed from the electrode pad areas when etching the passivation and therefore the coated coverslips are also representative of these processes. The insulating glass substrate itself represents the CMOS interlayer dielectrics that lie under the metallisation. It is on this basis that we justify that our metal coated coverslips are representative of the surface presented to cells by CMOS.

2.1 Porous alumina

The porous alumina morphologies chosen for investigation were guided by the literature outlined in Section 1, with pore pitches ranging from 17–206 nm. Porous alumina formed using low anodisation voltages has a high porosity (i.e. the ratio of pore area to surface area). The porosity of the substrates produced at higher voltages can be increased by a phosphoric acid pore-widening etch. This method was used to replicate better the higher porosity of substrates used in previous studies (Table 1). Anodisation was

Table 1 Manufactured porous alumina substrates and comparison with other studies

Substrate	Anodising voltage (V)	Mean pore pitch (nm)	Porosity prior to pore-widening (%)	Final porosity (%)
'17 nm'	10	17	63[a]	63
'34 nm'	20	34	29[a]	29
'52 nm'	30	52	24[a]	24
'69 nm'	40	69	22	59
'103 nm'	60	103	22	38
'138 nm'	80	138	14	32
'172 nm'	100	172	13	30
'206 nm'	120	206	14	35
Hoess et al. (2007) - 40 V (oxalic electrolyte)				48
Hoess et al. (2007) - 150 V (phosphoric electrolyte)				39
Karlsson et al. (2003)				45
Karlsson et al. (2004) - 20 nm pore diameter				45
Karlsson et al. (2004) - 200 nm pore diameter				47
Sapelkin et al. (2006) - pSi				28

[a] pores not widened

performed in a beaker containing the electrolyte with magnetic stirrer and platinum mesh cathode. A Keithley 236 Source-Measure Unit provided the potential. For potentials up to and including 60 V the anodisation was performed at 25°C in a 4 wt % phosphoric acid electrolyte. For potentials greater than 60 V, anodisation was performed at 10°C with the electrolyte diluted with 25% v/v ethanol to avoid localised burning and metal fusing. Pore widening was performed using 4 wt % phosphoric acid at 45°C. A scanning electron microscope (Hitachi S-4300) was used to check the surfaces produced. As discussed in Graham et al. (2009) the inter pore distance is difficult to measure where pore layout is disordered since pore diameter and spacing vary. However, by applying a model of hexagonally organised pores (which is the expected morphology for highly ordered porous alumina films), the inter-pore distance, d, is approximated by $A/(\sqrt{3}.n)^{½}$, where the image represents area, A, with number of pores, n.

Additionally, the formation of porous alumina using the phosphoric acid electrolyte (H_3PO_4) results in a monolayer of aluminium phosphate covering the surface (Davis et al. 1982; Wagh 2004). This $AlPO_4$ was selectively etched from the alumina using hydrochloric acid (32 wt% HCl, 20ºC, 60 s) (Ding et al. 2005; Williams et al. 2003).

2.1.1 Trapped charge and annealing

It has been shown that anodisation of aluminium results in trapped charges within the alumina, with negative charges at the alumina surface and positive charges at the metal/oxide interface (Lambert et al. 2002; Vrublevsky et al. 2007a). Strong surface charges may cause excessively strong interaction with adhesion proteins resulting in denaturation (i.e. cell damage). A 1 h anneal at 200ºC was performed which is stated by Vrublevsky et al. 2007b to ensure that trapped charge, 'completely disappears'. This anneal is also of sufficiently low temperature to avoid altering CMOS transistor characteristics and so is compatible with CMOS MEA fabrication. We have not verified that these anneal conditions do indeed depolarise the alumina completely but have chosen to include this prescribed step since the alternative is, on balance, more likely to leave strong surface charges that may prevent adhesion.

2.2 Cell culture

For evaluation of electrode biocompatibility and adhesion the choice of NG108-15 cell line was governed by proposed applications, ease of use and past experience. These mammalian neuronal cells are a hybrid between mouse neuroblastoma and rat glioma. The cells, being clonal, have the advantage of behaving more consistently in a given environment and are free from satellite cells that often accompany primary neurons (Bowden et al. 1999).

Cells were cultured in 50 ml flasks (Nunc, Thermo Fisher Scientific), each containing 9 ml of growth medium (Dulbecco's Modified Eagle's Medium (DMEM) with GlutaMax (2 mM L-glutamine, Gibco), 5% foetal calf serum (FCS, Invitrogen), HAT supplement (30 μM hypoxanthine, 0.12 μM aminopterine, 4.8 μM thymidine, Sigma), 10 units ml^{-1} Penicillin and 0.1 mg ml^{-1} Streptomycin (Sigma) and incubated at 37ºC, 10% CO_2. Passaging was performed with a 3:1 division when cells were approximately 60–70% confluent, or occasionally 2:1 when only 50–60% confluent.

2.2.1 Cell vitality protocol

Anodised coverslip substrates were cleaved into approximately six squares of area ~1.0 cm^2 using a diamond scribe. Corrosion at the cleaved faces of aluminium substrates was prevented by coating the edges with either a bioinert silicone sealant (732, Dow Corning) or varnish ('TRV', Electrolube, UK). Sterilisation of the substrates was performed in the laminar flow hood by submersing in ethanol for 30 min followed by air drying for 15 min. The substrates were subsequently moved to sterile 35 mm dishes onto which 2 ml of cells (at a density of 10,000 – 20,000 ml^{-1}) were plated out and incubated at 37ºC, 10% CO_2.

Growth medium was replaced after 24 h with plating medium (DMEM with GlutaMax (2 mM L-glutamine), 1% FCS, Sigma HT supplement (30 μM hypoxanthine, 4.8 μM thymidine), Penicillin-Streptomycin as above). The cells were then incubated for a further 3 days prior to measurements.

Density of cells was normalised across different runs using plain glass coverslip sections of ~1 cm^2 as a normalising control. Density of cells in each dish for a single run was regulated by using a micropipettor to dispense precisely 2.0 ml of cells to each dish.

Due to the opacity of the aluminium substrates, it was necessary to use a microscope with epi-illumination (SMZ1500, Nikon) but it was found that this gave insufficient contrast between the cell and the aluminium or alumina substrates. It was found that sufficient contrast could be established by staining with Methylene Blue (5% w/v) in buffer solution (Deionised water, NaCl 120 mM, KCl 3 mM, $MgCl_2$ 1.2 mM, $NaHCO_3$ 22.6 mM, Glucose 11.1 mM, HEPES 5 mM, $CaCl_2$ 2.5 mM, with pH adjusted to 7.36 using HCl or/and NaOH) and filtered. Dwell time was 45–60 min. Unwanted cells that had adhered to the underside of the transparent glass normalising controls were removed using cotton buds dampened with buffer solution.

Images were captured using a digital camera (Nikon D200, 7.31×10^6 pixels/m), and the cell count process automated using the open source 'Cell Profiler' software

(Carpenter et al. 2006). Cell identification was optimised by applying a red filter in Cell Profiler to emphasise the blue-coloured cells, therefore easily distinguishing them from the substrate image background (Fig. 2(a), (e), (f)). Comparison with manual cell counts showed good correlation as long as cells were not clumped.

The premise of the biocompatibility test was based on the null hypothesis that there is no difference between cell density (vitality) on the aluminium versus the porous alumina substrates.

2.3 Cell adhesion assay

We have developed a centrifugation assay that has the potential of applying larger shear stresses than a flow chamber (Hertl et al. 1984; Reyes and Garcıa 2003). For consistency with flow chamber assays, we propose studying shear rather than normal forces on the cells, with substrates therefore mounted in the same plane as centrifuge rotation. The acceleration, a, on a cell is given by:

$$a = \omega^2(r + x) \tag{1}$$

where r is the radius from centrifuge axis to inner edge of the substrate, x is the distance of a cell from the inner edge of the substrate, and ω is the rotational speed. With small substrates of approximately 1 cm length, $r >> x$ and so the relationship can be simplified to $a=\omega^2 r$. With centrifuge speeds expressed in revolutions per minute (rpm), and with $\omega = 2\pi(\text{rpm})/60$, the acceleration can be stated more usefully as:

$$a = \left(\frac{\pi.(rpm)}{30}\right)^2 r \tag{2}$$

This acceleration is often expressed as a relative centrifugal force (RCF), RCF$=a/g$, where $g=9.81$ ms^{-2}. If required, the shear force on a cell, F, can then be determined by the relationship:

$$F = v_{cell}(\rho_{cell} - \rho_{medium})a \tag{3}$$

where v_{cell} is the volume of a cell, ρ_{cell} the density of a cell, and ρ_{medium} the density of the medium. With a physiological medium of density $\rho_{medium}=1.00\times10^3$kg.m^{-3} and an estimated cell density $\rho_{cell}=1.07\times10^3$kg.m^{-3} (Reyes and

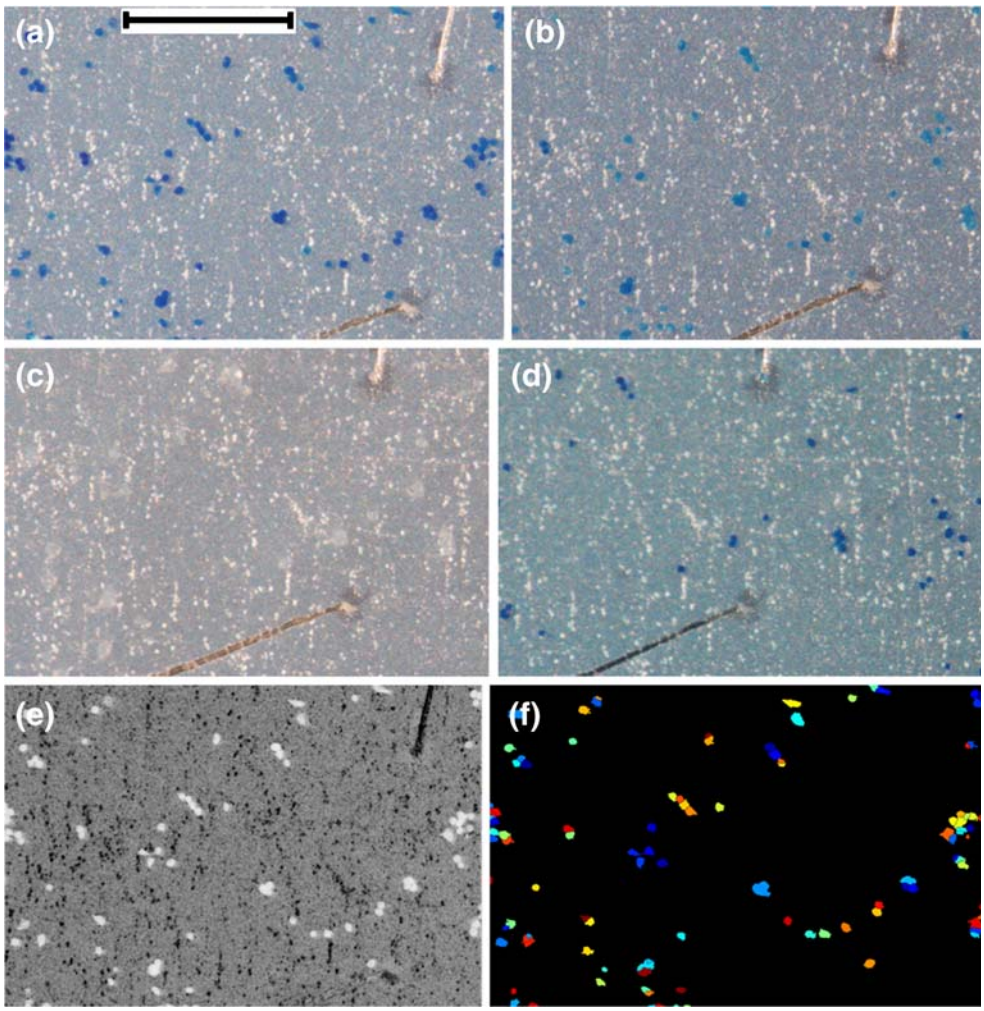

Fig. 2 Cell Count: (**a**) cells are clearly identifiable after initial staining, prior to centrifugation (porous alumina, '206 nm' pore pitch; scale bar is 400 μm). The white dots are remnants of aluminium metal that have not been anodised at the base of the porous alumina film. A vertical scratch at the top and a diagonal scratch at the bottom of the image were applied to this trial substrate as reference marks; (**b**) the same substrate area after centrifugation at 2000 rpm for 5 min and (**c**) after 8000 rpm for 5 min. The stain has leached and cells have become difficult to identify; (**d**) although many cells detach, restaining confirms that some cells remain adhered but had lost stain during centrifugation; (**e**) the blue-stained cells in image (a) are emphasised by applying a red filter in the 'Cell Profiler' software; (**f**) cells can then be correctly identified by 'Cell Profiler' image analysis

Garcıa 2003), it can be seen that the cell's effective weight in medium (i.e. the detachment force, F) is small compared with its weight in air, $v_{cell} \cdot \rho_{cell} \cdot g$. Centrifugation assays have been performed in air by Hertl et al. (1984) to increase the detachment force, but is undesirable here as the cells would no longer be in physiological conditions.

In order to create sufficient detachment forces, it was necessary to use high centrifuge speeds. A bucket rotor provides orthogonal rotation of tubes and therefore also gives simplicity of design but buckets are limited to relatively low rotation speeds. It was therefore necessary to design the centrifugation assay using a fixed angle rotor (Sigma 3 K-30 centrifuge; 6×50 ml angle rotor). Holders were designed to present the substrates in an almost horizontal position within the angled centrifuge rotor so that the centrifugal acceleration was primarily in line with the plane of the substrate and so creating a shear detachment force (Fig. 3).

The substrates were angled very slightly (< 3º) to prevent them from flipping up onto the sidewall of the holder during centrifugation. This angle reduced the shear force by only ~0.1% (i.e. 1 - cos 3°) and so an acceptable approximation was to consider the coverslips as horizontal.

The holder design was found to be adequate up to speeds of 18,000 rpm. Breakages occurred above this speed due to the entire weight of the substrate being transferred via its two outside corners. If required, higher speeds could be obtainable by designing a holder to distribute the weight along the entire outer edge of the glass.

Preliminary experiments using cells stained with methylene blue resulted in loss of stain from the cells during extended exposure to buffer. This was observed both in a flow chamber and low-speed (<4200 rpm) centrifuge. The fact that this phenomenon occurred in the flow chamber and at low centrifugation speeds suggested the problem was more likely to be diffusion of the stain back into the buffer rather than damage of cell membrane. This was also found to be the case in Hertl et al. (1984). Cells with leached stain were easily confused with detached cells during cell counts, but the problem was simply resolved by centrifugation in buffer containing methylene blue (5% w/v) instead of plain buffer (Fig. 2(a)–(d)). Centrifugation was performed at 20°C with the set speed maintained for 5 min. Ramping of centrifuge speed was controlled to avoid disturbance of substrates.

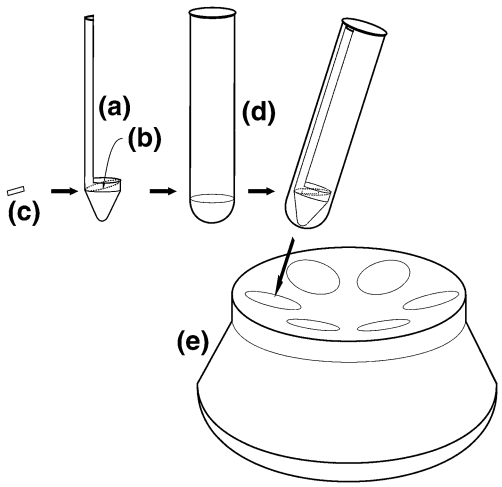

Fig. 3 Centrifugation assembly: The holder (**a**) is a modified universal tube, with one side cut away. The remaining segment of the side acts as a handle. The base of the universal is filled with resin (**b**) (Sylgard, Dow Corning) and allowed to set so that its surface is almost level when inserted in the angle rotor. The substrate (**c**) is loaded onto the holder and inserted into a polycarbonate centrifuge tube (**d**) containing stain

3 Results

Porous alumina substrates were prepared (Fig. 4) and evaluated by analysis of scanning electron microscope images using the open-source ImageJ software (Abramoff et al. 2004). The substrate characteristics are summarised in Table 1.

Cell vitality tests showed no significant difference between the aluminium control and any of the anodised substrates (Table 1 and Fig. 5).

For the adhesion assay, detachment of cells was treated using statistical methods for survival (Lee 1980). Data were fitted to a 3-parameter Weibull distribution, with a threshold of zero (i.e. no failing cells at 0 rpm since unadhered cells were removed during handling); the same Weibull shape parameter was applied to all substrates whilst maintaining an acceptable goodness of fit ($R^2 \geq 0.887$). Figure 6 shows these data as a percentage of cells detached as a function of centrifugation speed. The solid symbols represent experimental data while the lines represent the data fitted to the Weibull distributions. Each fit is shown as a set of three curves representing mean, upper confidence interval and lower confidence interval. A comparison of the curves of Fig. 6 was performed by ANOVA (Analysis of Variance) of the 50% cell detachment points, τ_{50} (Table 2 and Fig. 7). The 17 nm and 69 nm alumina substrates showed significantly poorer adhesion than the aluminium, whereas cells adhered significantly better to the 206 nm alumina compared to aluminium. The acceleration can be calculated using Eq. 2 and is shown as the second y axis in Fig. 5.

4 Discussion

4.1 Mode of electrode operation

Figure 8 shows a simplified electrical model for a single pore element, with an input to a high impedance amplifier

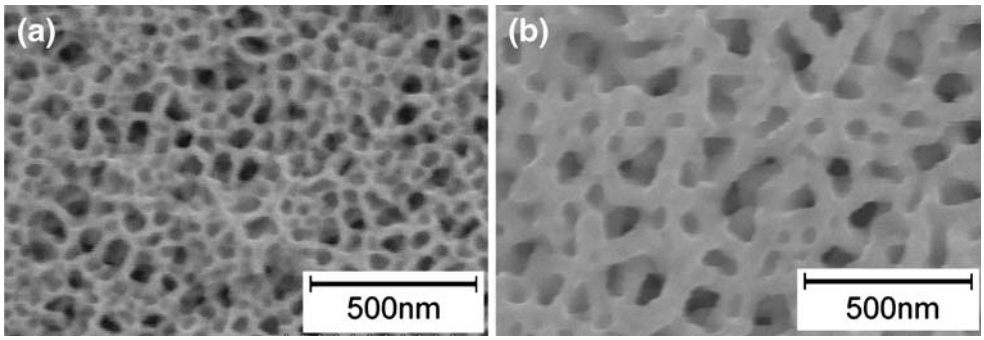

Fig. 4 Examples of porous alumina substrates: (**a**) anodised at 30 V; (**b**) anodised at 60 V prior to pore-widening

for recording. Stimulation is performed using a similar arrangement with the electrode potential determined by an amplifier output. The intracellular potential, v_{int}, is coupled to the electrode via the cell membrane impedance, c_m and r_m. The seal resistance element, r_s, represents the lateral leakage path from the extracellular space (cleft) below the cell membrane to the bath electrode (ground): maximising this resistance is critical to forming a good electrical junction between cell and electrode (Ingebrandt et al. 2005; Gleixner and Fromherz 2006; Voelker and Fromherz 2005). To achieve this, the height of the cleft must be minimised (Cohen et al. 2008). The resistance r_p represents the physiological medium in the pore and is small (compared with c_b and r_b) due to the relatively high conductivity of the medium (typically 10^3 S.m^{-1} (Gleixner and Fromherz 2006; Prasad and Quijano 2006)). A double layer impedance is formed at the solid-solution interface comprising capacitance c_d and resistance r_d. With characteristic action potential frequencies being in the order of 1 kHz, the magnitude of the impedance $(2\pi fc_d)^{-1}$ that results from the double layer capacitance typically dominates resistance r_d by a factor of 10^3 to 10^5 (Ouerd et al. 2007; Franks et al. 2006).

The anodic barrier layer impedance, c_b and r_b, at the base of the alumina pore governs the overall electrical characteristics of the film (van der Linden et al. 1990). This is initially of high impedance during pore formation but can be reduced by methods such as subsequent electrodeposition of a noble metal, by thinning the barrier oxide using a post-anodisation etch, by electrochemical thinning, or by almost completely anodising the aluminium thin film until the hemispherical barrier oxide deforms (Gould and Sadler 1983; Furneaux et al. 1989).

Additionally, it must be considered that the pore walls of insulating alumina do not contribute to the active area of the electrode and so the impedance of the basic porous electrode will always be greater than a planar metal surface. Electrodes with low porosity would therefore present a particularly large impedance. It is also expected that the lateral seal resistance of the cleft will scale with porosity due to lower impedance formed laterally across the electrolyte-filled pores. A poor seal resistance may therefore be anticipated for highly porous films. As discussed further in Graham et al. (2009), the above suggest a trade-off between good seal resistance and good coupling through the base of the pores and so extremes of porosity are likely to produce particularly poor electrical performance.

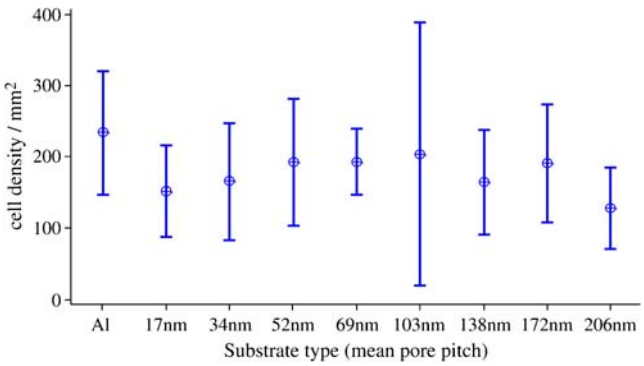

Fig. 5 Comparison of cell density on anodised substrates versus aluminium control (n=6, 3 runs), showing no significant differences between means (p=0.698). Error bars represent 95% confidence intervals. Glass controls were used to normalise cell density across runs

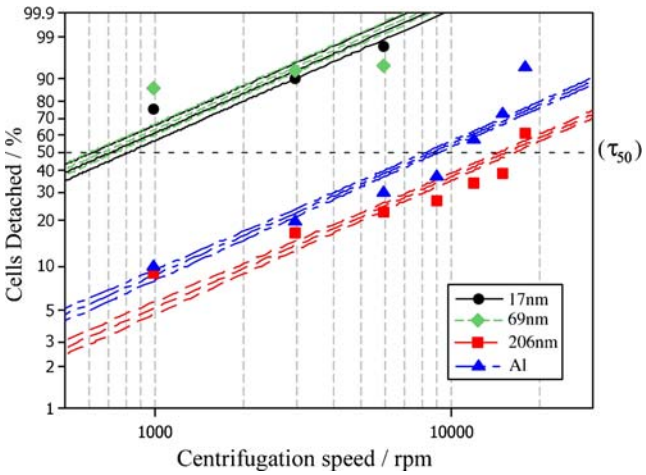

Fig. 6 Cell detachment profiles for 17 nm, 69 nm and 206 nm porous alumina and aluminium substrates (n=8, 4 runs). Data were arbitrarily censored. Curves are means and 95% confidence intervals for fits to Weibull distributions (threshold=0, shape=0.9381)

Table 2 τ_{50} and standard errors for porous alumina substrates and aluminium control

Substrate	τ_{50} / rpm	Standard Error (SE) at τ_{50} / rpm
Al	8779	231.8
17 nm	719	51.1
69 nm	676	35.2
206 nm	15662	487.2

4.2 Biocompatibility

The vitality assay showed that a porous alumina surface is biocompatible with mammalian neuronal cells. This agrees with other work describing alumina as bioinert (Ravaglioli and Krajewski 1992; Williams 1981). From the above results it is evident that pore pitch has no discernible effect on cell vitality. Conversely, the centrifugation adhesion assay demonstrated that pore pitch modulates the ability for neuronal cells to adhere to the surface. This corroborates Schneider et al. (2001) in finding that vitality is not a good indicator of adhesion.

4.3 Comparison with other quantitative studies of adhesion

The above results are in broad agreement with another study of long-term adhesion (Hertl et al. 1984) where Vero Green Monkey kidney (fibroblast-like) cells had a mean long-term detachment force that approached a maximum RCF of approximately 5000 after 25 h. However, the majority of other quantitative adhesion tests have assessed only short-term processes which are of little relevance in the context of an electrode.

An additional problem arises in comparing centrifugation results with other methods due to the difficulty in evaluating absolute detachment force: for example, the short-term (12 h) adhesion of NG108-15 cells on untreated glass was measured in Cargill et al. (1999) to have a mean detachment shear of 0.67 Nm^{-2} (6.7±0.23 $dyn.cm^{-2}$). From these data, the absolute detachment force on a single cell

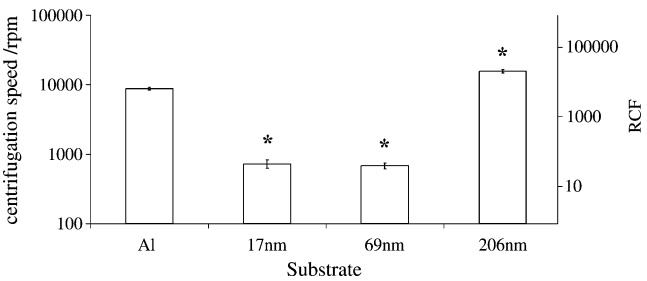

Fig. 7 Analysis of τ_{50} for aluminium control and porous alumina substrates (n=8, 4 runs) showing significant (*) differences (p<0.05). Error bars represent 95% confidence intervals

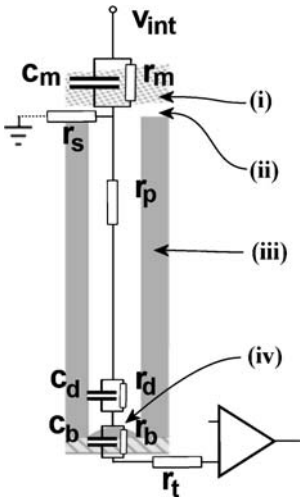

Fig. 8 Electrical model of a single electrode element: (i) cell membrane; (ii) cleft; (iii) pore wall; (iv) barrier oxide at pore base. Superimposed electrical elements are intracellular potential, v_{int}, membrane impedance, c_m and r_m, seal (cleft) resistance, r_s, pore resistance, r_p, double layer impedance c_d and r_d, barrier oxide impedance c_b and r_b, and electrode access resistance of the metal track, r_t

can be determined only if the surface area of the cell exposed to the moving fluid is known. This was attempted by Garcia et al. (1997) by using assumptions of cell morphology (that cells were spherical) and an estimate of 10% for the proportion of cell surface in contact with the substrate. However, this figure has latterly been shown to be too low, with the proportion more likely to range between 12–40% (mean of 32%) for HEK293 cells on uncoated glass (Sommerhage et al. 2008) and so demonstrates the difficulty in using such an estimate to quantify force. Similarly for centrifugation, calculation of detachment force via the aforementioned relationship (Eq. 3) would require the cell volume, v_{cell}, to be determined.

Comparison between fluid shear and centrifugation methods could be made via the relationship between cell volume and cell surface area, but this requires quantitative evaluation of cell morphology (i.e. degree of cell flattening) and cell contact area. Because of these difficulties, a quantitative comparison between shear and RCF data is likely to result in unacceptable inaccuracy and so has not been attempted.

4.4 Pore pitch

To explain the difference in adhesion of the smaller pore pitches (17 nm, 69 nm) compared to the larger pore pitch (206 nm) we considered porosity and morphology.

The porosity of a substrate surface is the ratio of pore area to surface area. Without pore-widening, smaller pore pitches such as the 17 nm and 69 nm substrates have higher porosities than substrates produced using higher voltages. Below a cell body a highly porous substrate will present mainly physiological medium (i.e. within the pores) and in these areas can provide no adhesion: cell adhesion molecules can bond only with the surface formed by the tops of the thin pore walls.

Secondly, it is conceivable that the morphology of the alumina could modulate adhesion, as noted in Karlsson et al. (2003) where cell processes were observed to enter the larger pores of 200 nm diameter, but not into pores of less than 100 nm — it was perceived that the larger pores may provide anchorage points.

Additionally, the native aluminium oxide clearly cannot present such anchorage yet we have shown it results in good adhesion. However, it might not be appropriate to make deductions regarding adhesion mechanism by direct comparison of the porous alumina and native oxide surfaces: for example, the stoichiometries of the artificial and native oxides are likely to differ; it is also conceivable that surface charge may be different even though we endeavoured to depolarise the alumina by the anneal step. Alternatively one could adopt a view that considers the planar native oxide surface as a porous alumina with zero porosity and zero pore diameter. In this case it would be valid to make deductions by comparing adhesion to native oxide and porous alumina substrates. In this scenario we would postulate that for our combination of neuronal cells and porous alumina, that it is the proportion of porous alumina surface (porosity) that modulates adhesion rather than surface morphology. However, since the mechanisms may differ between planar and porous surfaces this must remain an aspect of the work that is open for future discussion. Physical analysis of these cell-substrate interfaces may help identify the likely adhesion mechanisms and is planned as future work.

5 Conclusion

A modified CMOS electrode has been proposed based on a conductive porous alumina substrate that enhances electrochemical stability and maintains acceptable electrical performance. Porous alumina substrates were produced, controlling surface chemistry and trapped electrical charges. The substrates were shown to be biocompatible with NG108-15 neuronal cells. A novel centrifugation assay was developed to measure long-term cell adhesion strength of various porous alumina pore pitches versus a plain aluminium surface. Small pore pitches of 17 nm and 69 nm result in poor cell adhesion whereas a large pore pitch of 206 nm presents good adhesion with slightly better performance than the planar aluminium surface of an unmodified CMOS electrode. This work is of benefit in the design of low-cost CMOS electrodes using biocompatible porous alumina of optimum pore morphology.

Acknowledgements This work has been partly funded by the UK Engineering and Physical Sciences Research Council via a doctoral training grant.

References

M.D. Abramoff, P.J. Magelhaes, S.J. Ram, Biophoton. Int. **11**, 36 (2004)
S.C. Bayliss, L.D. Buckberry, P.J. Harris, M. Tobin, J. Porous Mater. **7**, 191 (2000). doi:10.1023/A:1009686704506
L. Berdondini, P.D. van der Wal, N.F. de Rooij, M. Koudelka-Hep, Sens. Actuator B-Chem. **99**, 505 (2004). doi:10.1016/j.snb.2003.12.078
E. Bogner, K. Dominizi, P. Hagl, E. Bertagnolli, M. Wirth, F. Gabor, Acta Biomater. **2**, 229 (2006). doi:10.1016/j.actbio.2005.10.006
P. Bongrand, in *Handbook of Biological Physics (Vol. 1)*, ed. by R. Lipowsky, E. Sackmann (Elsevier, Netherlands, 1995), p. 755
S.E.H. Bowden, A.A. Selyanko, J. Robbins, J. Physiol. **519**, 23 (1999). doi:10.1111/j.1469-7793.1999.0023o.x
R.D. Brinton, W. Sousou, M. Baudry, M. Thompson, T.W. Berger, in *Toward Replacement Parts for the Brain: Implantable Biomimetic Electronics as Neural Prostheses*, ed. by T.W. Berger, D. Glanzman (MIT, London, 2005)
R.S. Cargill, K.C. Dee, S. Malcolm, Biomaterials **20**, 2417 (1999). doi:10.1016/S0142-9612(99)00169-6
A.E. Carpenter, T.R. Jones, M.R. Lamprecht, C. Clarke, I.H. Kang, O. Friman et al., Genome Biol. **7**, R100 (2006)
A. Cohen, J. Shappir, S. Yitzchaik, M.E. Spira, Biosens. Bioelectron. **23**, 811 (2008)
G.D. Davis, T.S. Sun, J.S. Ahearn, J.D. Venables, J. Mater. Sci. **17**, 1807 (1982)
G.Q. Ding, M.J. Zheng, W.L. Xu, W.Z. Shen, Nanotechnology **16**, 1285 (2005)
J.W. Dini, *Electrodeposition: The Materials Science of Coatings and Substrates* (Noyes, Park Ridge, 1993)
J.P. Donoghue, A. Nurmikko, M. Black, L.R. Hochberg, J. Physiol. **579**, 603 (2007)
W. Franks, I. Schenker, P. Schmutz, A. Hierlemann, IEEE Trans. Biomed. Eng. **52**, 1295 (2006)
P. Fromherz, Physica E **16**, 24 (2003)
R.C. Furneaux, W.R. Rigby, A.P. Davidson, Nature **337**, 147 (1989)
N.D. Gallant, A.J. García, Methods Mol. Biol. **370**, 83 (2007)
A.J. Garcia, P. Ducheyne, D. Boettiger, Biomaterials **18**, 1091 (1997)
D.C. Giliberti, K.A. Anderson, K.C. Dee, J. Biomed. Mater. Res. Part B **62**, 422 (2002)
R. Gleixner, P. Fromherz, Biophys. J. **90**, 2600 (2006)
R.D. Gould, D.N. Sadler, Int. J. Electron. **54**, 21 (1983)
A.H.D. Graham, C.R. Bowen, J. Robbins, J. Taylor, Sens. Actuator B-Chem. (2009). doi:10.1016/j.snb.2009.01.050
F. Greve, S. Frerker, A. Greet Bittermann, C. Burkhardt, A. Hierlemann, H. Hall, Biomaterials **28**, 5246 (2007)
F. Heer, S. Hafizovic, T. Ugniwenko, U. Frey, W. Franks, E. Perriard, Biosens. Bioelectron. **22**, 2546 (2007)
W. Hertl, W.S. Ramsey, E.D. Nowlan, *In Vitro* Cell. Dev. Biol.-Plant **20**, 796 (1984)
A. Hoess, N. Teuscher, A. Thormann, H. Aurich, A. Heilmann, Acta Biomater. **3**, 43 (2007)
S. Ingebrandt, C.K. Yeung, M. Krause, A. Offenhäusser, Eur. Biophys. J. **34**, 144 (2005)
F. Johansson, M. Kanje, C.E. Linsmeier, L. Wallman, IEEE Trans. Biomed. Eng. **55**, 1447 (2008)
H. Kaper, H.J. Busscher, W. Norde, J. Biomater. Sci.-Polym. Ed. **14**, 313 (2003)
M. Karlsson, A. Johansson, L. Tang, M. Boman, Microsc. Res. Tech. **63**, 259 (2004)
M. Karlsson, E. Palsgard, P.R. Wilshaw, D. Silvio, Biomaterials **24**, 3039 (2003)
M. Kawahara, M. Kato, Y. Kuroda, Brain Res. Bull. **55**, 211 (2001)

J. Lambert, C. Guthmann, C. Ortega, M. Saint-Jean, J. Appl. Phys. **91**, 9161 (2002)
E.E. Leary Swan, K.C. Popat, C.A. Grimes, T.A. Desai, J. Biomed. Mater. Res. Part A **72A**, 288 (2005)
E.T. Lee, *Statistical Methods for Survival Data Analysis* (Lifetime Learning, Belmont, 1980)
S.P. Low, K.A. Williams, L.T. Canham, N.H. Voelcker, Biomaterials **27**, 4538 (2006)
A.H. Mayne, S.C. Bayliss, P. Barr, M. Tobin, L.D. Buckberry, Phys. Status Solidi A-Appl. Mat. **182**, 505 (2000)
K.A. Moxon, N.M. Kalkhoran, M. Markert, M.A. Sambito, J.L. McKenzie, J.T. Webster, IEEE Trans. Biomed. Eng. **51**, 881 (2004)
A. Ouerd, C. Alemany-Dumont, G. Berthomé, B. Normand, S. Szunerits, J. Electrochem. Soc. **154**, C593 (2007)
D.P. Perl, S. Moalem, in *Alzheimer's Disease: A Century of Scientific and Clinical Research*, ed. by G. Perry (IOS, Amsterdam, 2006)
P. Prasad, J. Quijano, Biosens. Bioelectron. **21**, 1219 (2006)
A. Ravaglioli, A. Krajewski, *Bioceramics: Materials, Properties, Applications* (Chapman & Hall, London, 1992)
J. Ressler, H. Grothe, E.R. Motrescu, B. Wolf, Eng Med. Bio. Soc., 2004. IEMBS '04. 26th Ann. Intl Conf. IEEE **1**, 2074 (2004)
C.D. Reyes, A.J. Garcıa, J. Biomed. Mater. Res. Part A **67**, 328 (2003)
A.G. Sabnis, *VLSI Reliability (VLSI Electronics Microstructure Science 22)* (Academic, San Diego, 1990)
A.V. Sapelkin, S.C. Bayliss, B. Unal, A. Charalambou, Biomaterials **27**, 842 (2006)
T.W. Schneider, H.M. Schessler, K.M. Shaffer, J.M. Dumm, L.A. Yonce, Biomed. Microdevices **3**, 315 (2001)
I. Schoen, P. Fromherz, Biophys. J. **92**, 1096 (2007)
F. Sommerhage, R. Helpenstein, A. Rauf, G. Wrobel, A. Offenhausser, S. Ingebrandt, Biomaterials **29**, 3927 (2008)
H. Sorribas, D. Braun, L. Leder, P. Sonderegger, L. Tiefenauer, J. Neurosci. Methods **104**, 133 (2001)
B. van der Linden, H. Terryn, J. Vereecken, J. Appl. Electrochem. **20**, 798 (1990)
S. Virtanen, I. Milošev, E. Gomez-Barrena, R. Trebše, J. Salo, Y.T. Konttinen, Acta Biomater. **4**, 468 (2008)
M. Voelker, P. Fromherz, Small **1**, 206 (2005)
I. Vrublevsky, A. Jagminas, J. Schreckenbach, W.A. Goedel, Electrochim. Acta **53**, 300 (2007a)
I. Vrublevsky, A. Jagminas, J. Schreckenbach, W.A. Goedel, Appl. Surf. Sci. **253**, 4680 (2007b)
A. Wagh, *Chemically Bonded Phosphate Ceramics: Twenty-First Century Materials with Diverse Applications* (Elsevier, London, 2004)
A.R. Walpole, E.P. Briggs, M. Karlsson, E. Pålsgård, P.R. Wilshaw, Mat.-wiss. u. Werkstofftech **34**, 1064 (2003)
D.F. Williams, *Biocompatibility of Clinical Implant Materials*, vol. 1 (CRC, Boca Raton, 1981)
K.R. Williams, K. Gupta, M. Wasilik, J. Microelectromech. Syst. **12**, 761 (2003)
B. Wolfrum, Y. Mourzina, F. Sommerhage, A. Offenhäusser, Nano Letters **6**, 453 (2006)
G. Wrobel, M. Holler, S. Ingebrandt, S. Dieluweit, F. Sommerhage, H.P. Bochem, A. Offenhausser, J. R. Soc. Interface **5**, 213 (2008)